

Synthesis, Redox, and Magnetic Properties of a Neutral, Mixed-Valent Heptanuclear Manganese Wheel with $S = 27/2$ High-Spin Ground State^{†,‡}

Rolf W. Saalfrank,^{*,§} Andreas Scheurer,^{*,§} Raju Prakash,[§] Frank W. Heinemann,[§] Takayuki Nakajima,^{||} Frank Hampel,[⊥] Roland Leppin,[#] Bernd Pilawa,[#] Holger Rupp,[⊗] and Paul Müller^{*,⊗}

Institut für Anorganische Chemie der Universität Erlangen-Nürnberg, Egerlandstraße 1, 91058 Erlangen, Germany, Department of Applied Chemistry, School of Science and Engineering, Waseda University, Okubo 3-4-1, Shinjuku-ku, Tokyo 169-8555, Japan, Institut für Organische Chemie der Universität Erlangen-Nürnberg, 91054 Erlangen, Germany, Physikalisches Institut, Universität Karlsruhe (TH), 76128 Karlsruhe, Germany, and Physikalisches Institut III der Universität Erlangen-Nürnberg, 91054 Erlangen, Germany

Received July 27, 2006

Reaction of lithium tetrachloromanganate(II) with *N*-*n*-butyldiethanolamine H_2L^3 (**3**) in the presence of LiH leads to the formation of wheel-shaped, mixed-valent heptanuclear, neutral complex $\{Mn^{II} \subset [Mn^{II}_2Mn^{III}_4Cl_6(L^3)_6]\}$ (**4**). The manganese wheel crystallizes in the triclinic space group $P\bar{1}$ as **4**·2CHCl₃ or **4**·3THF when either diethyl ether or *n*-pentane was allowed to diffuse into solutions of **4** in chloroform or tetrahydrofuran. The oxidation states of each manganese ion in **4**·2CHCl₃ or **4**·3THF were assigned on the basis of detailed symmetry, bond length, and charge considerations, as well as by the Jahn–Teller axial elongation observed for the manganese(III) ions, and were further supported by cyclic voltammetry. The analysis of the SQUID magnetic susceptibility data for complex **4**·2CHCl₃ showed that the intramolecular magnetic coupling of the manganese(II,III) ions is dominated by ferromagnetic exchange interactions. This results in an $S = 27/2$ ground-state multiplet at low magnetic field. At fields higher than 0.68 T, the energetically lowest state is given by the $m_S = 31/2$ component of the $S = 31/2$ multiplet due to the Zeeman effect. The ligand-field-splitting parameters were determined by anisotropy SQUID measurements on single crystalline samples along the crystallographic *x*, *y*, and *z* axes ($D = -0.055$ K, $E = 6.6$ mK) and by high-frequency electron spin resonance measurements on a polycrystalline powder of **4**·2CHCl₃ ($D = -0.068$ K, $E = 9.7$ mK). The resulting barrier height for magnetization reversal amounts to $U \approx 10$ K. Finally, 2DEG Hall magnetization measurements revealed that **4**·2CHCl₃ shows single-molecule magnet behavior up to the blocking temperature of about 0.6 K with closely spaced steps in the hysteresis because of the quantum tunneling of the magnetization.

Introduction

Single-molecule magnets (SMMs) function as single-domain magnetic particles below their blocking temperatures. The origin of the magnetization hysteresis of these complexes

is the anisotropy barrier $U \approx |D|S^2$ between the high-spin ground states $\pm S$ of one single molecule because of the zero-field splitting of the ground-state multiplet.¹ If the easy axes of magnetic anisotropy of all molecules in the crystal lattice are parallel aligned, macroscopic measurements reflect the properties of a single quantum chemical object. In order to use the properties of SMMs for technical applications, like data storage and quantum computation, larger blocking temperatures are desirable.² Thus, a major challenge in molecular magnetism is to synthesize compounds that possess a large spin S as well as a high ligand-field-splitting parameter D . Molecules with a maximum-spin economy

* To whom correspondence should be addressed. E-mail: saalfrank@chemie.uni-erlangen.de (R.W.S.), andreas.scheurer@chemie.uni-erlangen.de (A.S.), phm@physik.uni-erlangen.de (P.M.).

[†] Dedicated to Professor Ernst Anders on the occasion of his 65th birthday.

[‡] Chelate Complexes, Part 35. Part 34: ref 12o

[§] Institut für Anorganische Chemie der Universität Erlangen-Nürnberg.

^{||} Waseda University.

[⊥] Institut für Organische Chemie der Universität Erlangen-Nürnberg.

[#] Universität Karlsruhe (TH).

[⊗] Physikalisches Institut III der Universität Erlangen-Nürnberg.

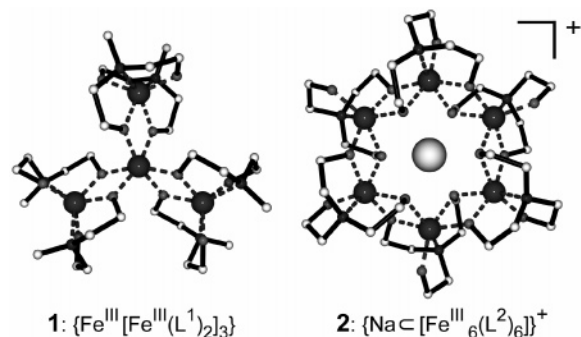


Figure 1. Ferric star **1** ($\text{H}_2\text{L}^1 = N$ -methyldiethanolamine; left) and cationic ferric wheel **2** ($\text{H}_3\text{L}^2 =$ triethanolamine; right).

simplify the theoretical description of these spin systems. By changing the nature of the metallic cations and the ligands, we aim to tune and control the ground-state spin of SMMs and attempt to optimize their magnetic properties. An example is the ferric star $\{\text{Fe}^{\text{III}}[\text{Fe}^{\text{III}}(\text{L}^1)_2]_3\}$ (**1**),^{3,4} which shows SMM behavior. The correlated ferric wheel $\{\text{Na}[\text{Fe}^{\text{III}}_6(\text{L}^2)_6]\}^+$ (**2**)⁵ with ground state $S = 0$ shows butterfly hysteresis because of a phonon bottleneck effect, that is just of partly molecular origin (Figure 1).

In this manuscript we report on the *neutral*, metal-centered, heptanuclear, mixed-valent $\{\text{Mn}_7\}$ wheel $\{\text{Mn}^{\text{II}}[\text{Mn}^{\text{II}}\text{Mn}^{\text{III}}_4\text{Cl}_6(\text{L}^3)_6]\}$ (**4**). We show that the intramolecular coupling in this complex is dominated by ferromagnetic interactions resulting in an $S = 27/2$ ground state with a blocking

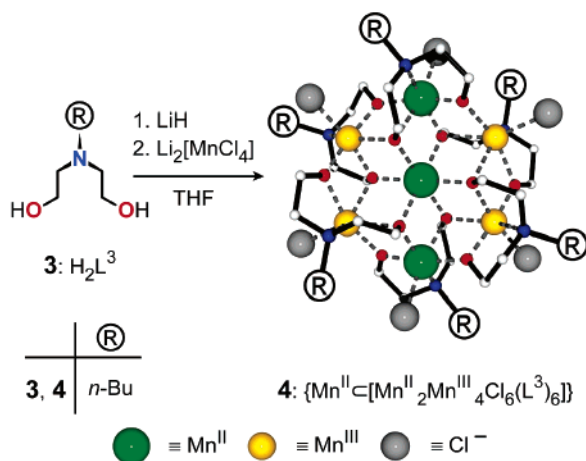
temperature of about 0.6 K. Furthermore, complex **4** exhibits SMM behavior as well as quantum tunneling of the magnetization (QTM).⁶ There are also reports on similar $\{\text{Mn}_7\}$ compounds like the *neutral* species $[\text{Mn}^{\text{II}}\text{C}[\text{Mn}^{\text{II}}_2\text{Mn}^{\text{III}}_4(\text{OME})_{12}(\text{dbm})_6]]$ (Hdbm = dibenzoylmethane)⁷ and $[\text{Mn}^{\text{II}}\text{C}[\text{Mn}^{\text{II}}_2\text{Mn}^{\text{III}}_4(\text{L}^4)_6]]$ ($\text{H}_3\text{L}^4 = N$ -(2-hydroxy-5-nitrobenzyl)iminodiethanol),⁸ the *dicationic* complexes $\{\text{Mn}^{\text{II}}\text{C}[\text{Mn}^{\text{II}}_3\text{Mn}^{\text{III}}_3(\text{HL}^2)_3(\text{L}^2)_3]\}^{2+}$ ($\text{H}_3\text{L}^2 =$ triethanolamine)⁹ and $\{\text{Mn}^{\text{II}}\text{C}[\text{Mn}^{\text{II}}_3\text{Mn}^{\text{III}}_3(\text{OH})_3\text{Cl}_3(\text{hmp})_9]\}^{2+}$ (Hhmp = 2-hydroxy-methylpyridine),¹⁰ and the *anionic* manganese wheels $\{\text{Mn}^{\text{II}}\text{C}[\text{Mn}^{\text{II}}_3\text{Mn}^{\text{III}}_3\text{Cl}_6(\text{L}^{1,5,6})_6]\}^-$ ($\text{H}_2\text{L}^{1,5,6} = N$ -methyl-, *N*-ethyl-, and *N*-benzyl-diethanolamine).¹¹ However, these complexes differ in the type of coupling from compound **4**, which represents one of the largest totally ferromagnetically coupled spin systems.

Results and Discussion

Synthesis. *Neutral* complex $\{\text{Mn}^{\text{II}}\text{C}[\text{Mn}^{\text{II}}_2\text{Mn}^{\text{III}}_4\text{Cl}_6(\text{L}^3)_6]\}$ (**4**) was generated in good yield under nitrogen in a one-pot reaction via self-assembly¹² in tetrahydrofuran (THF), starting from *N*-*n*-butyldiethanolamine H_2L^3 (**3**), lithium hydride, and lithium tetrachloromanganate(II) (Scheme 1). Workup on air and crystallization from chloroform or THF afforded the solvent containing black parallelepiped **4**·2CHCl₃ or **4**·3THF, respectively.

Description of Crystal Structures. X-ray crystallographic structure determinations of **4**·2CHCl₃ and **4**·3THF were

- (1) (a) Barbara, B.; Thomas, L.; Lionti, F.; Chiorescu, I.; Sulpice, A. *J. Magn. Magn. Mater.* **1999**, *200*, 167–181. (b) Gatteschi, D.; Sessoli, R.; Cornia, A. *Chem. Commun.* **2000**, 725–732. (c) Coronado, E.; Galán-Mascarós, J.-R.; Gómez-García, C.-J.; Ensling, J.; Gütllich, P. *Chem.—Eur. J.* **2000**, *6*, 552–563. (d) Sessoli, R.; Gatteschi, D. *Angew. Chem.* **2003**, *115*, 278–309; *Angew. Chem., Int. Ed.* **2003**, *42*, 268–297. (e) Wittick, L. M.; Murray, K. S.; Moubaraki, B.; Batten, S. R.; Spiccia, L.; Berry, K. J. *J. Chem. Soc., Dalton Trans.* **2004**, 1003–1011. (f) Murugesu, M.; Wernsdorfer, W.; Abboud, K. A.; Christou, G. *Angew. Chem.* **2005**, *117*, 914–918; *Angew. Chem., Int. Ed.* **2005**, *44*, 892–896. (g) Foguet-Albiol, D.; O'Brien, T. A.; Wernsdorfer, W.; Moulton, B.; Zaworotko, M. J.; Abboud, K. A.; Christou, G. *Angew. Chem.* **2005**, *117*, 919–923; *Angew. Chem., Int. Ed.* **2005**, *44*, 897–901. (h) Rumberger, E. M.; Shah, S. J.; Beedle, C. C.; Zakharov, L. N.; Rheingold, A. L.; Hendrickson, D. N. *Inorg. Chem.* **2005**, *44*, 2742–2752. (i) Murugesu, M.; Habrych, M.; Wernsdorfer, W.; Abboud, K. A.; Christou, G. *J. Am. Chem. Soc.* **2004**, *126*, 4766–4767.
- (2) Leuenberger, M. N.; Loss, D. *Nature* **2001**, *410*, 789–793.
- (3) (a) Saalfrank, R. W.; Bernt, I.; Chowdhry, M. M.; Hampel, F.; Vaughan, G. B. M. *Chem.—Eur. J.* **2001**, *7*, 2765–2769. (b) Saalfrank, R. W.; Scheurer, A.; Bernt, I.; Heinemann, F. W.; Postnikov, A. V.; Schünemann, V.; Trautwein, A. X.; Alam, M. S.; Rupp, H.; Müller, P. *J. Chem. Soc., Dalton Trans.* **2006**, 2865–2874. (c) Takács, A. F.; Neumann, M.; Postnikov, A. V.; Kuepper, K.; Scheurer, A.; Sperner, S.; Saalfrank, R. W.; Prince, K. C. *J. Chem. Phys.* **2006**, *124*, 044503/1–8.
- (4) See also: (a) Cornia, A.; Fabretti, A. C.; Garrisi, P.; Mortalò, C.; Bonacchi, D.; Gatteschi, D.; Sessoli, R.; Sorace, L.; Wernsdorfer, W.; Barra, A.-L. *Angew. Chem.* **2004**, *116*, 1156–1159; *Angew. Chem., Int. Ed.* **2004**, *43*, 1136–1139. (b) Accorsi, S.; Barra, A.-L.; Caneschi, A.; Chastanet, G.; Cornia, A.; Fabretti, A. C.; Gatteschi, D.; Mortalò, C.; Olivieri, E.; Parenti, F.; Rosa, P.; Sessoli, R.; Sorace, L.; Wernsdorfer, W.; Zoppi, L. *J. Am. Chem. Soc.* **2006**, *128*, 4742–4755 and references cited therein.
- (5) (a) Waldmann, O.; Koch, R.; Schromm, S.; Müller, P.; Bernt, I.; Saalfrank, R. W. *Phys. Rev. Lett.* **2002**, *89*, 246401/1–4. (b) Waldmann, O.; Koch, R.; Schromm, S.; Schüle, J.; Müller, P.; Bernt, I.; Saalfrank, R. W.; Hampel, F.; Balthes, E. *Inorg. Chem.* **2001**, *40*, 2986–2995. (c) Saalfrank, R. W.; Bernt, I.; Uller, E.; Hampel, F. *Angew. Chem.* **1997**, *109*, 2596–2599; *Angew. Chem., Int. Ed. Engl.* **1997**, *36*, 2482–2485.
- (6) Thomas, L.; Lionti, F.; Ballou, R.; Gatteschi, D.; Sessoli, R.; Barbara, B. *Nature* **1996**, *383*, 145–147.
- (7) Abbati, G. L.; Cornia, A.; Fabretti, A. C.; Caneschi, A.; Gatteschi, D. *Inorg. Chem.* **1998**, *37*, 3759–3766.
- (8) Koizumi, S.; Nihei, M.; Nakano, M.; Oshio, H. *Inorg. Chem.* **2005**, *44*, 1208–1210.
- (9) Pilawa, B.; Kelemen, M. T.; Wanka, S.; Geisselmann, A.; Barra, A. L. *Europhys. Lett.* **1998**, *43*, 7–12.
- (10) (a) Bolcar, M. A.; Aubin, S. M. J.; Folting, K.; Hendrickson, D. N.; Christou, G. *Chem. Commun.* **1997**, 1485–1486. (b) Harden, N. C.; Bolcar, M. A.; Wernsdorfer, W.; Abboud, K. A.; Streib, W. E.; Christou, G. *Inorg. Chem.* **2003**, *42*, 7067–7076.
- (11) Saalfrank, R. W.; Nakajima, T.; Mooren, N.; Scheurer, A.; Maid, H.; Hampel, F.; Trieflinger, C.; Daub, J. *Eur. J. Inorg. Chem.* **2005**, 1149–1153.
- (12) (a) Saalfrank, R. W.; Demleitner, B. In *Perspectives in Supramolecular Chemistry*; Sauvage, J. P., Ed.; Wiley-VCH: Weinheim, Germany, 1999; Vol. 5, pp 1–51. (b) Uller, E.; Demleitner, B.; Bernt, I.; Saalfrank, R. W. In *Structure and Bonding*; Fujita, M., Ed.; Springer: Berlin, 2000; Vol. 96, pp 149–175. (c) Caulder, D. L.; Raymond, K. N. *Acc. Chem. Res.* **1999**, *32*, 975–982. (d) Fujita, M. *Chem. Soc. Rev.* **1998**, *27*, 417–425. (e) Jones, C. J. *Chem. Soc. Rev.* **1998**, *27*, 289–299. (f) Hof, F.; Craig, S. L.; Nuckolls, C.; Rebek, J., Jr. *Angew. Chem.* **2002**, *114*, 1556–1578; *Angew. Chem., Int. Ed.* **2002**, *41*, 1488–1508. (g) Holliday, B. J.; Mirkin, C. A. *Angew. Chem.* **2001**, *113*, 2076–2098; *Angew. Chem., Int. Ed.* **2001**, *40*, 2022–2043. (h) Seidel, S. R.; Stang, P. J. *Acc. Chem. Res.* **2002**, *35*, 972–983. (i) MacGillivray, L. R.; Atwood, J. L. *Angew. Chem.* **1999**, *111*, 1080–1096; *Angew. Chem., Int. Ed.* **1999**, *38*, 1018–1033. (j) Barea, E.; Navarro, J. A. R.; Salas, J. M.; Quirós, M.; Willermann, M.; Lippert, B. *Chem.—Eur. J.* **2003**, *9*, 4414–4421. (k) Winpenny, R. E. P. In *Perspectives in Supramolecular Chemistry*; Sauvage, J. P., Ed.; Wiley-VCH: Weinheim, Germany, 1999; Vol. 5, pp 193–223. (l) Cutland, A. D.; Malkani, R. G.; Kampf, J. W.; Pecoraro, V. L. *Angew. Chem.* **2000**, *112*, 2801–2803; *Angew. Chem., Int. Ed.* **2000**, *39*, 2689–2691. (m) Oshio, H.; Hoshino, N.; Ito, T.; Nakano, M.; Renz, F.; Gütllich, P. *Angew. Chem.* **2003**, *115*, 233–235; *Angew. Chem., Int. Ed.* **2003**, *42*, 223–225. (n) Watton, S. P.; Fuhrmann, P.; Pence, L. E.; Lippard, S. J.; Caneschi, A.; Cornia, A.; Abbati, G. L. *Angew. Chem.* **1997**, *109*, 2917–2919; *Angew. Chem., Int. Ed. Engl.* **1997**, *36*, 2774–2776. (o) Prakash, R.; Saalfrank, R.; Maid, H.; Scheurer, A.; Heinemann, F. W.; Trautwein, A. X.; Böttger, L. H. *Angew. Chem.* **2006**, *118*, 6017–6022; *Angew. Chem., Int. Ed.* **2006**, *45*, 5885–5889.

Scheme 1. Synthesis of Heptanuclear Mixed-Valent Manganese Wheel 4

carried out at low temperatures.^{13–16} According to these analyses, the $\{\text{Mn}_7\}$ core of these complexes is principally isostructural with idealized S_6 symmetry (Figure 2, top). Therefore, only the structure of $4 \cdot 2\text{CHCl}_3$ is discussed in detail. The manganese wheel $4 \cdot 2\text{CHCl}_3$ crystallizes in the triclinic space group $P\bar{1}$, and the unit cell consists of one independent molecule with two molecules of chloroform. The wheels are packed in the crystal, most simply, with all of the molecules piled in parallel forming columnar strands (Figure 2, bottom). In the crystal, the *neutral* metalla-coronate

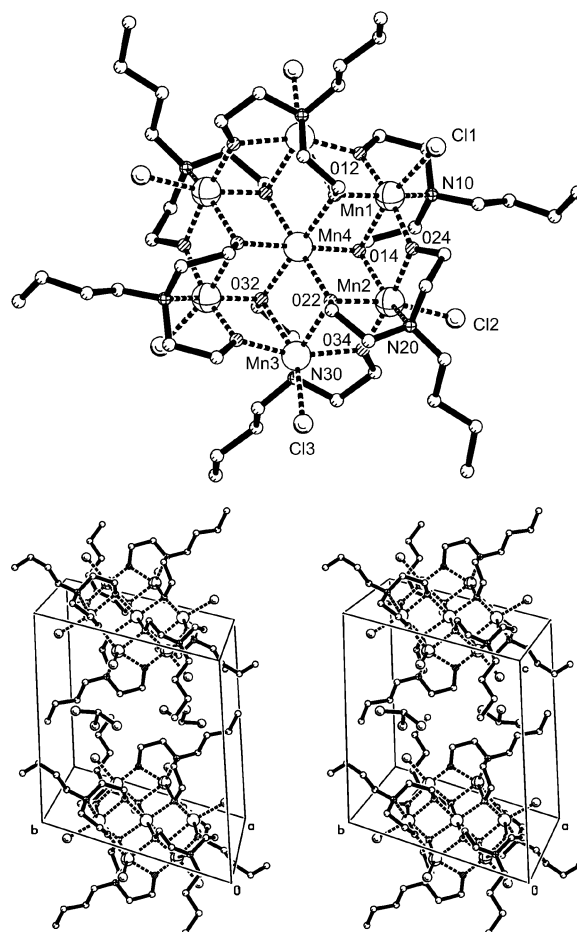


Figure 2. Top: PLUTON presentations of the molecular structure of complex $4 \cdot 2\text{CHCl}_3$ with the numbering of the Mn centers and coordinating atoms. View along the idealized molecular S_6 axis, neglecting the valency of the manganese centers. Bottom: Stereo presentation of the crystal packing of complex $4 \cdot 2\text{CHCl}_3$. Disorder of the *n*-butyl chain on $\text{Mn}1/1'$ and of solvent molecules as well as the hydrogen atoms was omitted for clarity. C, shaded; N, net; O, diagonal; Cl, segment; Mn^{II} , empty; Mn^{III} , cross.

is present as a Mn^{II} -centered, six-membered ring of four Mn^{III} and two Mn^{II} ions. Viewed along the S_6 axis, the peripheral manganese ions of centrosymmetric **4** are located in the corners of a regular hexagon. The distorted octahedral coordination sphere of the manganese ions is composed of one N and one Cl^- donor as well as two $\mu_2\text{-O}^-$ and two $\mu_3\text{-O}^-$ donors. The doubly deprotonated *N*-*n*-butyldiethanolamine acts as a tetratopic tridentate ligand which links four manganese ions via oxygen bridges.

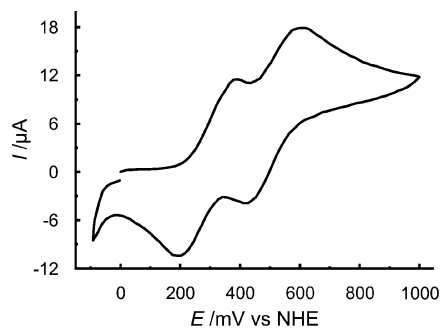
Detailed symmetry, bond length, and charge considerations of **4** require for the periphery a 2Mn^{II} , 4Mn^{III} oxidation state description and a Mn^{II} ion in the center (mixed-valent complex). The oxidation states of $\text{Mn}3/3'$ are assigned on the basis of the longer average $\text{Mn}-\text{O}$, $\text{Mn}-\text{N}$, and $\text{Mn}-\text{Cl}$ bond lengths as Mn^{II} ions compared with the bond lengths at $\text{Mn}1/1'$ and $\text{Mn}2/2'$ (Table 1). The mean distance d_θ at the Mn^{III} centers is equal to 2.110 Å, whereas at the peripheral Mn^{II} center, a mean distance $d_\theta = 2.262$ Å is found. In addition, the presence of a Jahn–Teller (JT) axial elongation at $\text{Mn}1/1'$ and $\text{Mn}2/2'$, as expected for a high-spin d^4 ion in near-octahedral geometry, clearly identifies those as Mn^{III} ions. For both Mn^{III} centers, O14 is in one of

- (13) Crystal data for $\{\text{Mn}^{\text{II}}\text{C}[\text{Mn}^{\text{III}}_2\text{Mn}^{\text{III}}_4\text{Cl}_6(\text{L}^3)_6]\}$ (**4**): $4 \cdot 2\text{CHCl}_3$; $\text{C}_{48}\text{H}_{102}\text{-Cl}_6\text{Mn}_7\text{N}_6\text{O}_{12} \cdot 2\text{CHCl}_3$, $M = 1791.37$ g mol $^{-1}$; crystal dimensions $0.30 \times 0.30 \times 0.20$ mm 3 ; triclinic, space group $P\bar{1}$, $a = 11.8080(2)$ Å, $b = 13.3640(3)$ Å, $c = 13.7280(3)$ Å, $\alpha = 70.2460(10)^\circ$, $\beta = 67.2800(10)^\circ$, $\gamma = 71.3640(10)^\circ$, $V = 1835.50(7)$ Å 3 ; $Z = 1$; $F(000) = 921$, $\rho_{\text{calcd}} = 1.621$ g cm $^{-3}$; Nonius KappaCCD diffractometer, Mo K α radiation ($\lambda = 0.71073$ Å); $T = 173(2)$ K; graphite monochromator; Θ range [deg] $2.24 < \Theta < 27.52$; section of the reciprocal lattice, $-15 \leq h \leq 15$, $-17 \leq k \leq 17$, $-17 \leq l \leq 17$; of 16 000 measured reflns, 8428 were independent and 6997 with $I > 2\sigma(I)$; linear absorption coefficient 1.658 mm $^{-1}$. The structure was solved by direct methods using SHELXS-97 and refined with all data (426 parameters) by full-matrix least-squares on F^2 using SHELXL97; all non-hydrogen atoms were refined anisotropically; $R1 = 0.0367$ for $I > 2\sigma(I)$ and $wR2 = 0.1033$ (all data); largest peak (0.862 e Å $^{-3}$) and hole (-0.821 e Å $^{-3}$).^{14a,b,15} Disorder: C18/C18' = 66:33, CHCl $_3$ 50:50. $4 \cdot 3\text{THF}$: $\text{C}_{48}\text{H}_{102}\text{Cl}_6\text{Mn}_7\text{N}_6\text{O}_{12} \cdot 3\text{THF}$, $M = 1768.95$ g mol $^{-1}$; crystal dimensions $0.28 \times 0.19 \times 0.12$ mm 3 ; triclinic, space group $P\bar{1}$, $a = 11.531(1)$ Å, $b = 13.297(2)$ Å, $c = 13.464(2)$ Å, $\alpha = 70.160(7)^\circ$, $\beta = 81.607(4)^\circ$, $\gamma = 89.674(6)^\circ$, $V = 1918.9(4)$ Å 3 ; $Z = 1$; $F(000) = 925$, $\rho_{\text{calcd}} = 1.531$ g cm $^{-3}$; Nonius KappaCCD diffractometer, Mo K α radiation ($\lambda = 0.71073$ Å); $T = 100(2)$ K; graphite monochromator; Θ range [deg] $3.03 < \Theta < 28.00$; section of the reciprocal lattice: $-15 \leq h \leq 15$, $-17 \leq k \leq 17$, $-17 \leq l \leq 17$; of 52 554 measured reflns, 9252 were independent and 6780 with $I > 2\sigma(I)$; linear absorption coefficient 1.385 mm $^{-1}$. The structure was solved by direct methods and refined with all data (508 parameters) by full-matrix least-squares on F^2 using SHELXTL NT 6.12; all non-hydrogen atoms were refined anisotropically; $R1 = 0.0301$ for $I > 2\sigma(I)$ and $wR2 = 0.0818$ (all data); largest peak (0.467 e Å $^{-3}$) and hole (-0.415 e Å $^{-3}$).^{14c,15} Disorder: C6/C6' = 48:52 and C8/C8' = 52:48; all of the solvent molecules (three THF) are disordered.
- (14) (a) Sheldrick, G. M.; Krüger, C.; Goddard, P. *Crystallographic Computing 3*; Oxford University Press: Oxford, 1985; p 175. (b) Sheldrick, G. M. *SHELXL-97: Program for Crystal Structure Refinement*; University of Göttingen: Göttingen, Germany, 1997. (c) *SHELXTL NT 6.12*; Bruker AXS, Inc.: Madison, WI, U.S.A., 2002.
- (15) CCDC 271730 [$(4) \cdot 2\text{CHCl}_3$] and CCDC 271408 [$(4) \cdot 3\text{THF}$] contain the supplementary crystallographic data for this paper. These data can be obtained free of charge from the Cambridge Crystallographic Data Centre via www.ccdc.cam.ac.uk/data_request/cif.
- (16) For further details compare with information in Supporting Information.

Table 1. Selected Interatomic Distances for the Oxidation State Determination of the Peripheral Manganese Centers in **4**·2CHCl₃^a

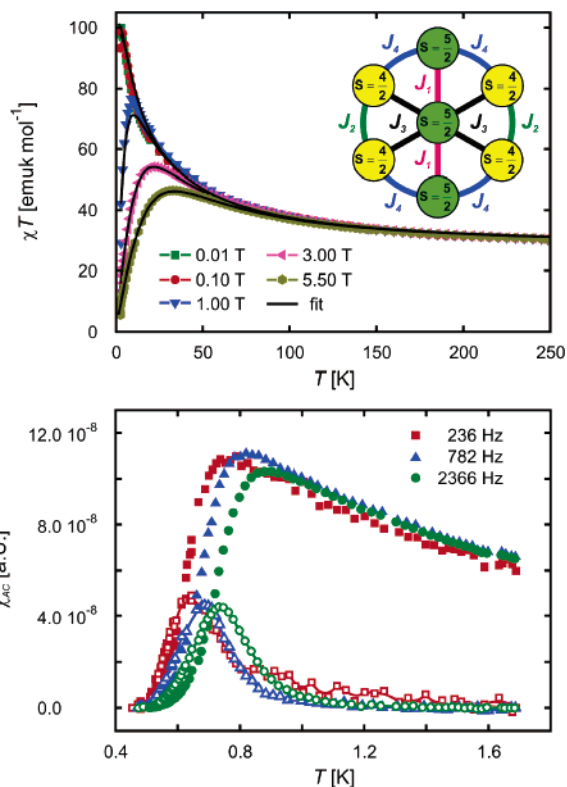
	d [Å]		d [Å]		d [Å]
Mn(1)–O(12)	1.880(2)	Mn(2)–O(14)	2.179(2)	Mn(3)–O(12)#1	2.141(2)
Mn(1)–O(14)	2.234(2)	Mn(2)–O(22)	2.061(2)	Mn(3)–O(22)	2.264(2)
Mn(1)–O(24)	1.950(2)	Mn(2)–O(24)	1.955(2)	Mn(3)–O(32)	2.320(2)
Mn(1)–O(32)#1	1.994(2)	Mn(2)–O(34)	1.872(2)	Mn(3)–O(34)	2.167(2)
Mn(1)–N(10)	2.135(2)	Mn(2)–N(20)	2.337(2)	Mn(3)–N(30)	2.274(2)
Mn(1)–Cl(1)	2.4273(7)	Mn(2)–Cl(2)	2.2905(7)	Mn(3)–Cl(3)	2.4083(6)
d_{O}	2.103	d_{O}	2.116	d_{O}	2.262
	Mn(1) = Mn ^{III}		Mn(2) = Mn ^{III}		Mn(3) = Mn ^{II}

^a Mn–heteroatom distances, indicating a JT axial elongation, are highlighted in bold.

**Figure 3.** CV of **4**; scan rate $\nu = 100$ mV s⁻¹.

the axially elongated positions. These data confirm for **4**·2CHCl₃ and **4**·3THF¹⁶ a ring of alternating one Mn^{II} and two Mn^{III} ions, each, with a Mn^{II} ion in the center.

Cyclic Voltammetry. The cyclic voltammogram (CV) of **4** exhibits two quasi-reversible redox waves at $E_{1/2} = 286$ and 516 mV, which are assigned to the successive one-electron oxidations of the two Mn^{II} ions located at the periphery of the ring (Figure 3).^{17,18} As usual, oxidation of the central Mn^{II} ion is not observed within the applied potential.^{11,19,20} In this context, the CV of **4** is compared with the analogous neutral indium–manganese wheel {Mn^{II}C[Mn^{II}₂–In^{III}₄Cl₆(L⁶)₆]} that has an identical core structure as **4**, but with four In^{III} ions at the periphery.²⁰ The CV of the latter complex measured under identical conditions also exhibited two one-electron redox waves in the positive potential range ($E_{1/2} = 330$ and 531 mV), but with a slightly more positive $E_{1/2}$ compared to **4**. In successive-scan experiments, both redox processes of **4** are diffusion-controlled (peak currents linearly proportional to the square root of the scan speeds) and revealed complete reversibility over several successive cycles. The large potential displacement (several hundred millivolts) between the individual oxidations indicates that a strong electronic coupling exists in solution between the crystallographically equivalent manganese ions, whereas in a non-coupled system, a simultaneous one potential twofold oxidation would have been expected. These findings are in

**Figure 4.** Top: DC susceptibility of **4**·2CHCl₃ in the temperature range above and below 2 K, respectively. We obtained an excellent fit of the experimental data with the following parameters: $g = 2.06$, $J_1 = 14.3$ K, $J_2 = -0.9$ K, $J_3 = -2.6$ K, $J_4 = 6.2$ K. Bottom: AC susceptibility of **4**·2CHCl₃, temperature dependence of the real (full symbols) and imaginary components (empty symbols) of the magnetic susceptibility measured at three frequencies of the alternating magnetic field.

good agreement with an alternating ring of one Mn^{II} and two Mn^{III} ions with one Mn^{II} ion in the center proposed by bond length and JT elongation studies.

Magnetic Susceptibility Studies. The direct current (DC) susceptibility of {Mn^{II}C[Mn^{II}₂Mn^{III}₄Cl₆(L³)₆]} **4**·2CHCl₃ was measured at different magnetic fields on polycrystalline samples in the range of 2.0–300 K using a MPMS-7 SQUID magnetometer. In order to analyze the intramolecular coupling between the Mn ions, the five DC susceptibility curves of the temperature dependence of χT at different magnetic fields in the range of 0.01–5.5 T were fitted simultaneously using a Heisenberg Hamiltonian including a Zeeman term (Figure 4, top). At least a set of three coupling parameters ($J_{\text{Mn(II)}-\text{Mn(II)}}$, $J_{\text{Mn(III)}-\text{Mn(III)}}$, and $J_{\text{Mn(II)}-\text{Mn(III)}}$) are necessary to describe the different couplings of the spins of the mixed-valent manganese centers. However, this set was insufficient to reproduce the experimental data. Therefore, a set of four

- (17) (a) Gagné, R. R.; Koval, C. A.; Lisinsky, G. C. *Inorg. Chem.* **1980**, *19*, 2854–2855. (b) Gritzner, G.; Kuta, J. *Pure Appl. Chem.* **1984**, *56*, 461–466.
- (18) Bard, A. J.; Faulkner, L. R. *Electrochemical Methods, Fundamentals and Applications*; Wiley: New York, 1980.
- (19) See also: (a) Ruben, M.; Rojo, J.; Romero-Salmero, F. J.; Uppadine, L. H.; Lehn, J.-M. *Angew. Chem.* **2004**, *116*, 3728–3747; *Angew. Chem., Int. Ed.* **2004**, *43*, 3644–3662. (b) Zhao, L.; Matthews, C. J.; Thompson, L. K.; Heath, S. L. *Chem. Commun.* **2000**, 265–266.
- (20) Saalfrank, R. W.; Prakash, R.; Maid, H.; Hampel, F.; Heinemann, F. W.; Trautwein, A. X.; Böttger, L. H. *Chem.–Eur. J.* **2006**, *12*, 2428–2433.

coupling parameters, distinguishing between the central and the peripheral coupling (Figure 4, top inset), were used (eq 1). This parameter set is also justified because of the observed differences in distances and angles of the peripheral and central coupling paths.

$$H_{\text{HB}} = \sum_{i=1}^7 g\mu_{\text{B}}\mu_0 S_i H + J_1 S_1 S_2 + J_1 S_1 S_3 + J_3 S_1 S_4 + J_3 S_1 S_5 + J_3 S_1 S_6 + J_3 S_1 S_7 + J_2 S_4 S_6 + J_2 S_5 S_7 + J_4 S_2 S_4 + J_4 S_2 S_5 + J_4 S_3 S_6 + J_4 S_3 S_7 \quad (1)$$

We obtained an excellent fit of the experimental data with the following parameters: $g = 2.06$, $J_1 = 14.3$ K, $J_2 = -0.9$ K, $J_3 = -2.6$ K, and $J_4 = 6.2$ K. Complex $4 \cdot 2\text{CHCl}_3$ shows an interplay between dominating ferromagnetic and weak antiferromagnetic intramolecular interactions resulting in an $S = 27/2$ ground state closely neighbored by excited spin states. In case of an applied magnetic field higher than 0.27 T, the $m_S = 29/2$ component of the first excited $S = 29/2$ multiplet gives the energetically lowest state because of the Zeeman effect. Finally, for applied magnetic fields larger than 0.68 T, the $m_S = 31/2$ component of the second excited $S = 31/2$ multiplet yields the energetically lowest state. The complex $4 \cdot 2\text{CHCl}_3$ shows different magnetic coupling than previously investigated similar complexes,^{7–10} in which antiferromagnetic intramolecular interactions played a more decisive role.

Alternating current (AC) susceptibility measurements in the low-temperature range, 0.45–2.0 K, reveal superparamagnetism (Figure 4, bottom). Assuming one relaxation time τ of the magnetization, we can determine the temperature dependence of τ from the maxima of the imaginary susceptibility by the condition $\omega\tau = 1$. From the maxima of $\chi''(\omega)$ (Figure 4, bottom) one finds a thermally activated relaxation (eq 2)

$$\tau = \tau_0 \exp(\Delta E/k_{\text{B}}T) \quad (2)$$

with $\tau_0 = (10 \pm 8) \times 10^{-11}$ s and $\Delta E/k_{\text{B}} = 10.0 \pm 0.5$ K.

SQUID and High-Frequency Electron Spin Resonance (ESR) Measurements. The magnetic moment of single crystals along the crystallographic x , y , and z axes was measured in the range of 0.0–5.5 T at 1.8 K. The magnetization curves confirm that the energetically lowest state is given by the $m_S = 31/2$ component of the $S = 31/2$ multiplet for fields larger than 0.68 T (Figure 5, top). Thus, we used the giant spin model of $S = 31/2$ in order to approximate the zero-field-splitting parameters. The corresponding Hamiltonian incorporating the Zeeman term and the second-order zero-field-splitting terms is given by eq 3,

$$H = g\mu_{\text{B}}\mu_0 S H + D S_z^2 + E(S_x^2 - S_y^2) \quad (3)$$

where g is the Landé factor, μ_{B} is the Bohr magneton, H is the applied magnetic field, D is the axial anisotropy constant, E is the transverse anisotropy constant, and S_x , S_y , and S_z are the components of the spin operator S . A two parameter fit of the three magnetization curves along the crystallographic x , y , and z axes gives $D = -0.055$ K and $E =$

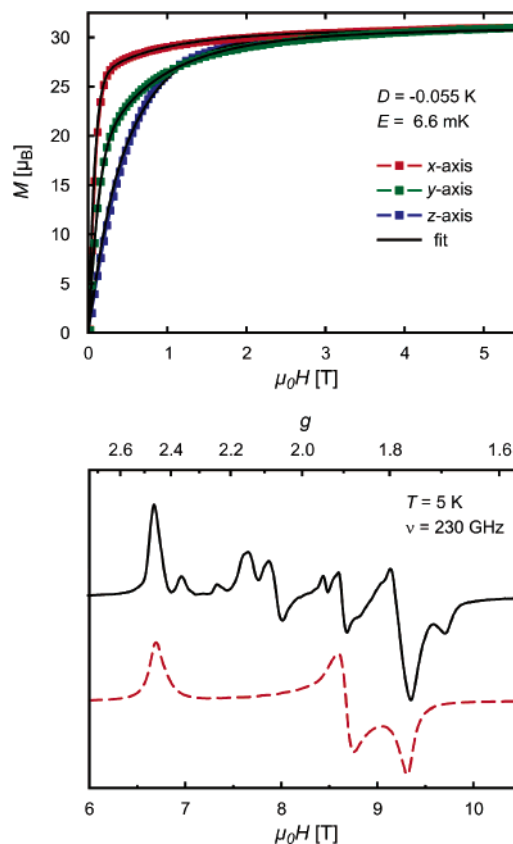


Figure 5. Top: SQUID measurements of $4 \cdot 2\text{CHCl}_3$ (dotted line) at 1.8 K and the two parameter fit (solid black lines) of the three magnetization curves along the x , y , and z directions. Bottom: Measured (solid line) and calculated (dashed line) ESR spectrum of a powder sample of $4 \cdot 2\text{CHCl}_3$ at $T = 5$ K and $\nu = 230$ GHz (for details see text).

6.6 mK. Although this is only a rough approximation due to the closely neighbored excited multiplets, we obtained an excellent fit. For low magnetic fields (<0.27 T), the resulting barrier height for magnetization reversal is $U = |D|S^2 = 10.02$ K. This corresponds exactly to the value we obtained from AC susceptibility measurements. The crossing fields due to the zero-field splitting are given by $H_n = \pm nD/g\mu_{\text{B}}$ for $n = 0, 1, 2, \dots$ ^{1a} Thus, the separation between adjacent anti-level crossings of $4 \cdot 2\text{CHCl}_3$ is only about $D/g\mu_{\text{B}} = 41$ mT.

High-frequency ESR measurements have been performed on a polycrystalline powder pellet of $4 \cdot 2\text{CHCl}_3$ at 95 and 230 GHz. The spectra have been recorded at several temperatures ranging from 5 to 20 K. The separation between the spectral lines is the same at 95 and 230 GHz. This indicates that the zero-field splitting is so small that the spectrum is dominated by the Zeeman effect, when the applied field B is larger than ~ 2 T. Figure 5 (bottom) shows the spectrum recorded at 5 K and 230 GHz. The large peak at the low-field side of the spectrum indicates a negative D parameter. The simulation of the experimental spectra has been performed using a program that calculates the matrix of the Hamiltonian (eq 3), for each sampled value and orientation of the magnetic field, and then diagonalizes this matrix. The spin $S = 31/2$ determined for the saturation magnetization and $g = 2.0$ has been used for the calculation. In agreement with the static magnetization measurements,

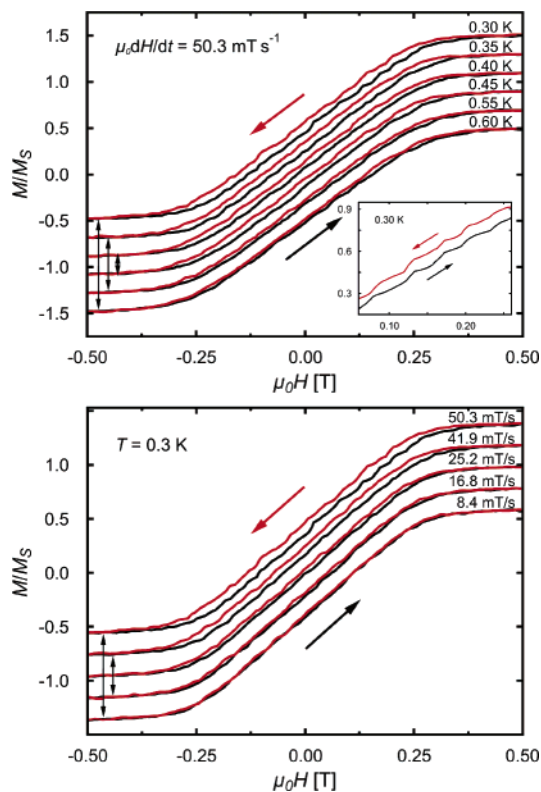


Figure 6. Hysteresis loops for single crystals of **4**·2CHCl₃ at the indicated temperatures (top) and the indicated sweep rates (bottom). Inset: the enlarged part of magnetization curve shows weakly pronounced steps slightly above the measurement resolution, which are caused by QTM at the numerous closely spaced avoided-level crossings.

it is not possible to simulate the spectrum with a pure axial zero-field splitting. The calculated curve in Figure 5b was obtained with the parameters $D = -0.068$ K, $E = 9.7$ mK, and $T = 5$ K. The D and E values are somewhat larger than those obtained from the fit of the magnetization measurements. This might indicate that the D and E parameters determined by the magnetization measurements are averaged over the lowest spin states. The simulation cannot reproduce all of the observed peaks of the spectrum. This might indicate that the powder pellet used for the measurements does not provide an isotropic powder average. Some of the characteristic features of the measured spectrum can be reproduced simply by restricting the averaging of the field orientations in the simulation routine.

Hall-Sensor Magnetization Measurements. Magnetization measurements were performed on single crystals of **4**·2CHCl₃, using a 2DEG GaAs/GaAlAs Hall sensor.²¹ A weakly pronounced hysteresis of the magnetization was observed below a blocking temperature of about 0.6 K (Figure 6, top). The width of the hysteresis decreases with increasing temperature and decreasing sweep rate as expected for a SMM (Figure 6, top and bottom). The shape of the hysteresis looks different compared to other SMMs because of the weak, easy axis anisotropy. Enhanced magnetic relaxation due to QTM at the numerous closely spaced

avoided-level crossings, H_n , strongly decreases the width of the hysteresis. It was shown by Wernsdorfer et al. that, despite the spin-parity effect, a half-integer spin system will also undergo tunneling at zero external field as a result of environmental degrees of freedom, such as hyperfine and dipolar couplings or a small intermolecular superexchange interaction.²² Additional level crossings caused by the neighbored excited multiplets and very weak intermolecular interactions might result in additional tunneling transitions between the fields H_n .

Conclusions

In summary, starting from manganese(II) salt and *N*-*n*-butyldiethanolamine, we formed a mixed-valent, neutral wheel of $\{\text{Mn}^{\text{II}}\text{C}[\text{Mn}^{\text{II}}_2\text{Mn}^{\text{III}}_4\text{Cl}_6(\text{L}^3)_6]\}$ (**4**). The molecular structures of **4**·2CHCl₃ and **4**·3THF were solved by single crystal X-ray structure determination. In **4**, four Mn^{III} ions in the periphery are arranged in pairs alternating with one Mn^{II} ion, each, with a Mn^{II} ion encapsulated in the center. The multistep one-electron redox reactions of **4** were studied by cyclic voltammetry. Magnetic studies of **4**·2CHCl₃ revealed a dominating ferromagnetic intramolecular coupling between the Mn ions resulting in a high-spin ground state of $S = 27/2$. At fields larger than 0.68 T, the energetically lowest state is given by the $m_S = 31/2$ component of the $S = 31/2$ multiplet because of the Zeeman effect. All previously investigated $\{\text{Mn}_7\}$ complexes with a similar coupling scheme showed only a ground state of $S \leq 22/2$ because of the dominating antiferromagnetic coupling. Thus, the specific ligand environment of the $\{\text{Mn}_7\}$ system **4**·2CHCl₃ must be responsible for the dominating ferromagnetic coupling. Complex **4**·2CHCl₃ exhibits SMM behavior up to the blocking temperature of about 0.6 K. Characteristic steps in the hysteresis due to QTM have been observed. Unlike other SMMs, the avoided level crossings in this case are closely spaced because of the relative small easy axis anisotropy, which results in the observed small width of the hysteresis.

Experimental Section

General Remarks. Unless stated otherwise, all reactions and manipulations were carried out under nitrogen using standard Schlenk techniques. Metal salts and H₂L³ (**3**) were used as obtained from Aldrich or Fluka. All solvents were purified and dried according to standard procedures. CVs were recorded with EG&G potentiostat PAR model 264A and a conventional three-electrode assembly consisting of a glassy carbon working electrode and Pt reference and counter electrodes. Solutions, CH₂Cl₂ [10^{-3} M]; supporting electrolyte, $[(n\text{-Bu})_4\text{N}][\text{PF}_6]$ [10^{-1} M]; internal standard, ferrocene. $E(\text{Fc}/\text{Fc}^+) = +410$ mV versus a normal hydrogen electrode;¹⁷ scan speeds, 25–200 mV s⁻¹; $T = 20$ °C. The reversibility of the voltammograms and the number of electrons involved in the redox processes were determined as described in the literature.¹⁸

Synthesis. Preparation of $\{\text{Mn}^{\text{II}}\text{C}[\text{Mn}^{\text{II}}_2\text{Mn}^{\text{III}}_4\text{Cl}_6(\text{L}^3)_6]\}$ (4**).** *N*-*n*-Butyldiethanolamine H₂L³ (**3**) (0.274 g, 1.7 mmol) was added

(21) Geim, A. K.; Dubonos, S. V.; Lok, J. G. S.; Grigorieva, I. V.; Maan, J. C.; Hansen, L. T.; Lindelof, P. E. *Appl. Phys. Lett.* **1997**, *71*, 2379–2381.

(22) (a) Wernsdorfer, W.; Bhaduri, S.; Boskovic, C.; Christou, G.; Hendrickson, D. N. *Phys. Rev. B* **2002**, *65*, 180403/1–4. (b) Wernsdorfer, W.; Chakov, N. E.; Christou, G. *Phys. Rev. Lett.* **2005**, *95*, 037203/1–4.

to a suspension of LiH (0.032 g, 4 mmol) in anhydrous THF (75 mL). After stirring this suspension for 1 h at room temperature (rt), a solution of $\text{Li}_2[\text{MnCl}_4]$ (4.00 mL, 2 mmol, 0.5 M) in THF was added dropwise, and the reaction mixture was stirred for 4 d at rt. The inhomogeneous reaction mixture was filtered on air, the THF solution was evaporated to dryness, and the resulting black precipitate was extracted with CHCl_3 (100 mL). Concentration, filtration, and vapor diffusion of Et_2O into the CHCl_3 solution afforded black crystals of $\mathbf{4}\cdot 2\text{CHCl}_3$. However, in this case, *n*-pentane was allowed to directly diffuse into the THF mother liquor, and black crystals suitable for X-ray structure analysis of $\mathbf{4}\cdot 3\text{THF}$ were obtained. Yield: 240 mg (47%) black crystals from chloroform/ Et_2O . Mp: >220 °C dec. IR (KBr): $\tilde{\nu} = 2961, 2910, 2864, 1455, 1378, 1247, 1073, 1052, 1034, 984, 919, 892, 749 \text{ cm}^{-1}$. FAB-MS (3-NBA): m/z (%) = 1552 (5) $[\text{Mn}_7\text{Cl}_6(\text{L}^3)_6]^+$, 1517 (9) $[\text{Mn}_7\text{Cl}_5(\text{L}^3)_6]^+$, 1482 (8) $[\text{Mn}_7\text{Cl}_4(\text{L}^3)_6]^+$, 1357 (12) $[\text{Mn}_7\text{Cl}_5(\text{L}^3)_5]^+$, 1198 (27) $[\text{Mn}_7\text{Cl}_5(\text{L}^3)_4]^+$, 928 (74) $[\text{Mn}_5\text{Cl}_5(\text{L}^3)_3]^+$, 732 (100) $[\text{Mn}_5\text{Cl}_4(\text{L}^3)_2]^+$. Anal. Calcd for $\text{C}_{51}\text{H}_{105}\text{Cl}_{15}\text{Mn}_7\text{N}_6\text{O}_{12}$ (mol wt = 1910.78): C, 32.06; H, 5.54; N, 4.40. Found: C, 32.02; H, 5.75; N, 4.39.

Acknowledgment. This work was supported by the Deutsche Forschungsgemeinschaft Sa 276/27-1–2, SFB 583, GK 312, SPP 1137, the Bayerisches Langzeitprogramm Neue Werkstoffe, and the Fonds der Chemischen Industrie. T.N. thanks the *Alexander von Humboldt* Stiftung for a postdoctoral fellowship. The generous allocation of premises and cyclic voltammetric facilities by Prof. Dr. K. Meyer and Dr. M. Moll, respectively, at the Institut für Anorganische Chemie (Universität Erlangen-Nürnberg) is gratefully acknowledged.

Supporting Information Available: X-ray crystallographic files in CIF format for complexes $\mathbf{4}\cdot 2\text{CHCl}_3$ and $\mathbf{4}\cdot 3\text{THF}$ and the molecular structure, crystal packing, and table containing the selected interatomic distances for the oxidation state determination of the manganese centers of $\mathbf{4}\cdot 3\text{THF}$. This material is available free of charge via the Internet at <http://pubs.acs.org>.

IC0614059